Antimicrobial properties of sulphur-enriched, hydrophilic MoS_2 nano/microparticles and heterostructured Pd/MoS_2/Ti coatings

R. Žalnėravičius[1], M. Ragelytė[1], V. Klimas[1], G. Grincienė[1], R. Karpicz[1], A. Ramanavičius[1], A. Jagminas[1]
[1]Center for physical siences and technology, Sauletekio av. 3, LT-10222 Vilnius, Lithuania
E-mail: rokas.zalneravicius@ftmc.lt

FIZINIŲ IR TECHNOLOGIJOS MOKSLŲ CENTRAS

Introduction

Recently, graphene-like two-dimensional molybdenum disulphide-based nanomaterials, especially their single or few-layered forms, usually named nanosheets (MoS_2-ns) or nanoknifes, have received considerable attention as a promising antimicrobial agent. However, most previous studies indicate that without functionalization with other antimicrobial agents such as Ag, Ti_3C_2MXene, graphene oxide (GO) [1, 2], etc., the antimicrobial efficiency of MoS_2 is low and needs further improvements. In this study, the MoS_2-based nano/microparticles and coatings were synthesized through a simple, one-step hydrothermal approach without any other additives. The fabricated materials exhibited relatively small ($\Delta\theta$ =18.7 ± 2.5º) contact angle, resulting in their prominent hydrophilic properties, possibly caused due to sulphur-enriched MoS_2 composite as evidenced by TG/DTA–MS analysis. Such nanostructures can exhibit a better adhesion of biomolecules, thus facilitating the interaction between them, as confirmed by highly effective antimicrobial action (Fig. 1). The present study examines the antimicrobial properties of hydrophilic, sulphur-enriched MoS_2 nano/microparticles as well as MoS_2-based coatings against various humans' pathogenic bacteria such as *S. enterica*, *P. aeruginosa*, *E. coli*, *S. aureus* (MRSA), *M. luteus*, and two *Candida* fungi, in particular *C. parapsilosis*, *C. krusei*. The MoS_2-ns (40 µg mL^{-1}) showed over 90 % killing efficiency against *S. aureus* MRSA bacteria and two *Candida* fungi within 24 h of exposure. Surprisingly, the petal-like MoS_2 microstructures and heterostructured MoS_2/Ti and Pd/MoS_2/Ti coatings also possess high antimicrobial potency and could be considered a promising antimicrobial agent and thus deserve further studies. The MoS_2-induced intracellular reactive oxygen species (ROS) production was evidenced by measuring the standard DCF dye fluorescence.

Characterization of the MoS_2 NPs, petal-like MoS_2 spheres

The structural analysis of the as-grown product was performed using TEM and AFM techniques. Morphology investigations of MoS_2-ns revealed that these NPs have a narrow size distribution between 0.8 and 2.8 nm with an average diameter of 1.8 nm (Fig. 1 b, d). TEM results match well those determined by atomic force microscopy, which showed that these NPs were exfoliated to a few-layered material with a narrow size distribution (Fig. 1 c). The spherical structure of black MoS_2 powder with petal-like surface design (as presented in Fig. 1 e) was synthesized by a hydrothermal approach. SEM image depicted that bulk MoS_2 are mainly spherical with average diameters of 1.5–2.5 µm and their surface is uniformly covered with differently oriented leaflets. In order to prove their lamellar structure, the individual leaflet edges were assessed by TEM. Figure 1 f indicate lamellar morphology with dominant interlayer spacing approximately equal to 0.62 Å attributable to (002) plane of MoS_2.

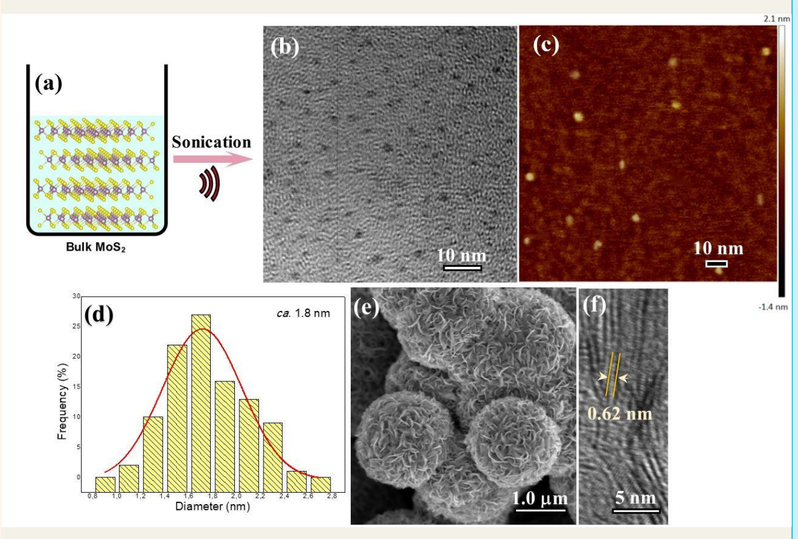

Fig. 1. TEM (b) and AFM (c) images of nanosheets obtained by ultrasonic exfoliation procedure (a) of hydrothermally synthesized MoS_2 powder. Histogram of size distribution acquired from multiple TEM images is shown in (d). SEM image of hydrothermally produced MoS_2 black powder resembles petal-like spheres (e). In (f), HR-TEM image of nanoplatelets edges.

Morphology and phase investigation of nanoplatelet MoS_2/Ti and Pd/MoS_2/Ti coatings

The cross-section SEM photographs show that the thickness of MoS_2/Ti coatings after 5 h autoclaving approximated to 410 nm (see Insets in Fig. 2 b). The as-formed electrodes were further decorated with Pd NPs *via* electroless deposition method. The morphology of this deposits (Fig. 2 b, c) confirms the existence of plenty spherical-shaped Pd crystallites scattered on the MoS_2/Ti surface. The deposited Pd NPs are uniformly distributed, have an average size of 24 nm and cover approximately 15.7 % of the surface's area. Direct evidence of the deposited noble metals and their loading was observed by EDX and ICP-OES analyses. From EDX investigations, the deposited crystallites could be attributed to palladium. The content of noble metals was only 1.42 atomic percentage with the 4.96 µg cm^{-2} loading density of Pd NPs on the surface of MoS_2.

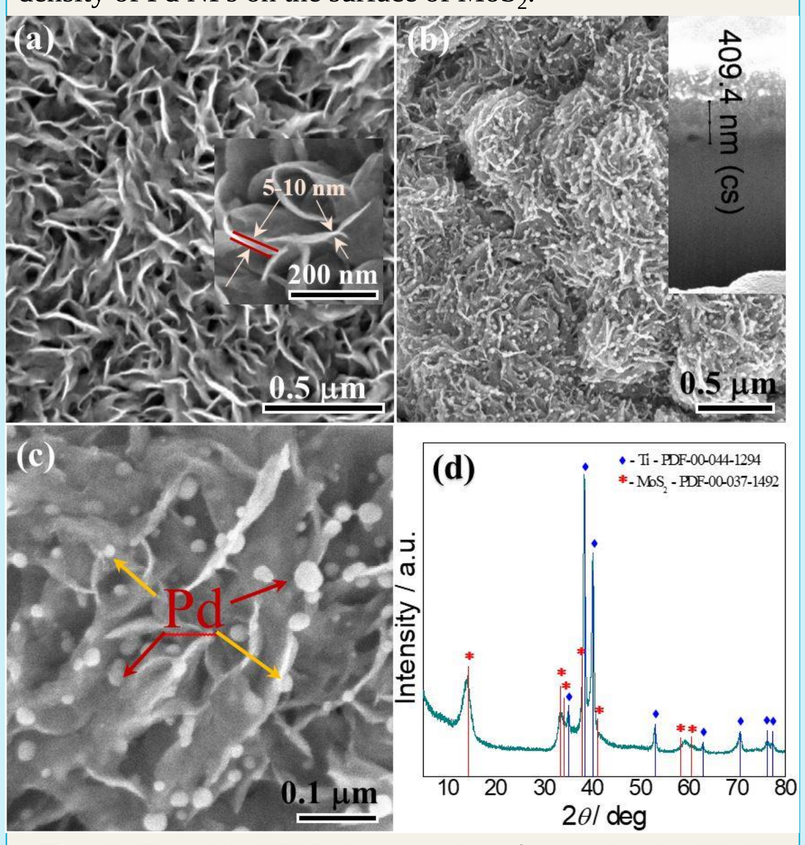

Fig. 2. Top-side SEM photographs of nanoplatelet MoS_2 films fabricated on the Ti substrate by hydrothermal treatment from an aqueous solution of 5.0 mM ammonium heptamolybdate and 90 mM thiourea at 220 ºC for 10 h before (a) and after chemical decoration with palladium NPs at different magnification (b, c). In (d) XRD patterns of MoS_2/Ti species. Insets: top-side SEM image of leaflets edge at highest magnification and cross-section SEM image of MoS_2 species on Ti substrate.

TG/DTA-MS investigations

In order to determine the phase purity and composition of as-grown, petal-like MoS_2 powders, the TG/DTA-MS investigations were further performed herein. The evolution of sulphur under an argon atmosphere (Fig. 3 curve 8) can be linked with the presence of different chemical state of sulphur. Since the production of MoS_2 occurs through an intermediate MoS_3 stage and generation of free sulphur, this evaporation can be related to nanometric-sized sulphur residues or MoS_3 phase decomposition, which starts to releasing sulphur from 200 ºC.

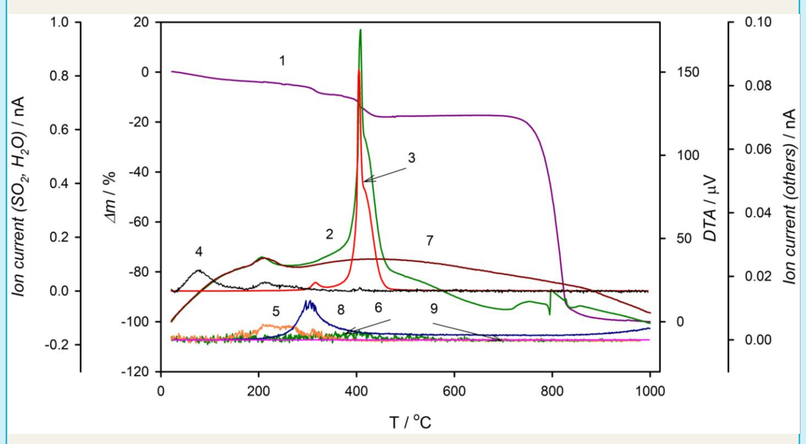

Fig. 3. TG/DTA-MS analysis of hydrothermally synthesized MoS_2 powder. TG (1) and DTA curves recorded under synthetic air (2), and argon (7) atmospheres. Curves 3, 4, 5, 6 and 8, 9 present ion current of gaseous species decomposed in synthetic air (SO_2, H_2O, NO/NO_2, CO_2) and argon (S_2, CS_2), respectively.

Antimicrobial activity of MoS_2-based materials

Antimicrobial activity of MoS_2-ns, petal-like MoS_2 and MoS_2-based coatings were evaluated *via* serial broth dilution method. The results obtained in this study clearly establishing that MoS_2-ns possess the bactericidal or fungicidal potential against all tested microorganism and are summarised in Fig 4. The microorganism survival histograms clearly show the concentration-dependent antimicrobial activity of the synthesized MoS_2-ns against all tested bacteria and yeast. It is evident from the results that MoS_2-ns were highly effective towards the inactivation of bacteria and surprisingly, two species of *Candida* yeast.

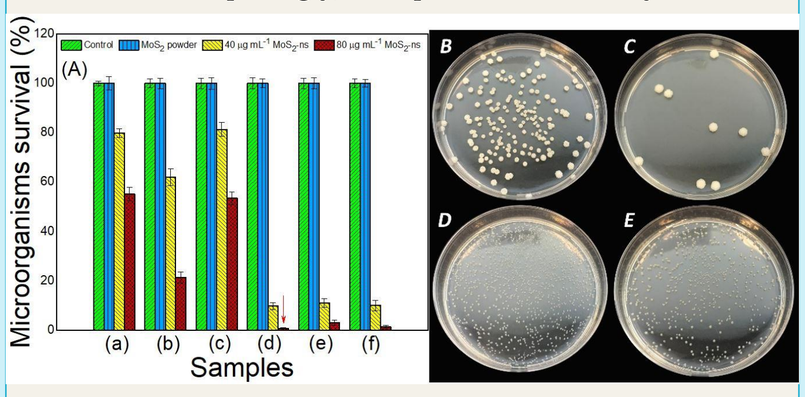

Fig. 4. Antimicrobial potency of MoS_2-ns against prokaryotic *E. coli* (a), *P. aeruginosa* (b), *S. enterica* (c), *S. aureus* MRSA (d) and eukaryotic *C. parapsilosis* (e), *C. krusei* (f) microorganisms after 24 h treatment at 37 and 28 ºC, respectively. Photographs are showing the quantification of *C. krusei* (top row) and *E. coli* (bottom row) CFU growth inhibition induced by MoS_2-ns. The leftmost Petri dishes (B, D) present control samples.

Determination of ROS

The overproduction of ROS occurs as a consequent of MoS_2-ns interaction with bacteria membrane, which turns the antioxidant defence mechanism and, thus induce oxidative stress, therefore the cells are unable to maintain the physiological redox-regulated process. Generation of ROS initiate the oxidation of proteins, induce the lipid peroxidation, cause DNA damage and could be responsible for genotoxic effects.

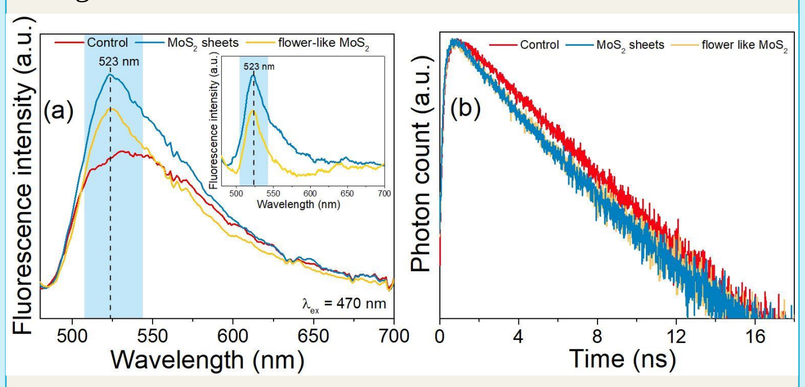

Fig. 5. Fluorescence spectra (a) and fluorescence decay kinetics (b) of DCF dye that was intracellular de-esterified by Gram-negative *Pseudomonas aeruginosa* bacteria and oxidized by ROS after exposure with MoS_2-ns and flower-like MoS_2 particles for 2 hours at 37 ºC under 150 rpm. Insets: The fluorescence spectra after subtraction of bacteria fluorescence.

The obtained photoluminescence emission peak at 523 nm wavelength is related to DCE dye fluorescence, which was obtained after exposure of *P. aeruginosa* bacteria with MoS_2 nano/microparticles (Fig. 5 a). It is notable that due to bacteria autofluorescence, a control sample of bacteria solution demonstrated the one broad emission peak with a maximum at 530 nm wavelength, however after subtraction of this spectrum the DCF dye emission peaks become more apparent (Fig. 5 Insets). The lifetime of *P. aeruginosa* bacteria photoluminescence exhibit two exponential decay and exceeds the average relaxation time (τave) equal to 4 ns (Fig. 5 b). However, after exposure to DCF and MoS_2 particles, the fluorescence decay kinetics changed, resulting in shorter τave value of 3.4 and 3.5 ns. These results suggest that MoS_2 nano/microparticles induce the intracellular ROS generation, thus cause the oxidation of DCFDA dye to highly fluorescence DCF compound that was detected herein.

Acknowledgements

This research was funded by the European Social Fund under the No 09.3.3-LMT-K-712-19-0155 "Development of Competences of Scientists, other Researchers and Students through Practical Research Activities" measure.